ADVANCED BIOSYSTEMS
www.adv-biosys.com

# Incorporation of Terbium into a Microalga Leads to Magnetotactic Swimmers

*Giulia Santomauro,* Ajay Vikram Singh, Byung-Wook Park, Mohammadreza Mohammadrahimi, Pelin Erkoc, Eberhard Goering, Gisela Schütz, Metin Sitti, and Joachim Bill*

**Swimming microorganisms have been shown to be useful for the propulsion of microrobotic devices due to their self-powered motion. Up to now, mainly bacteria, e.g., magnetotactic bacteria (MTB), are investigated as biohybrid microrobots. But biocompatibility studies of MTB regarding medical utilizations are still lacking. Moreover, MTB require special culture conditions for their stability, which also might limit their usage for biomedical applications. Herein, a cytocompatible, highly motile microswimmer is presented from a microalga, *Chlamydomonas reinhardtii*, which has the capacity to carry large loads. *C. reinhardtii* cells are magnetized by incorporating terbium. The following analyses reveal an induced magnetic moment of a magnetized *C. reinhardtii* cell of $1.6 \times 10^{-11}$ emu, comparable to its counterparts used as magnetotactic microrobots. The magnetized algae are able to align to the field lines of an applied uniform magnetic field, guiding them to swim in a directional motion. In addition, *C. reinhardtii* cells and human cells show mutual biocompatibility, indicating that the algae cells are noncytotoxic. Furthermore, the magnetized microalgae reported here are easy to track in the human body by luminescence imaging tools due to their innate autofluorescence performance and photoluminescence of the incorporated $Tb^{3+}$. Thus, terbium-incorporated microalgae are promising candidates for magnetically steerable biohybrid microrobots.**

## 1. Introduction

In recent years, microrobots have generated significant attention due to their broad potential applications in medicine.[1] Since they are minimally invasive and can move through hard-to-access or unprecedented regions inside the human body, they can serve as wireless transporters and drug delivery devices in specific local regions.[2–4] One of the main challenges in the development of untethered microrobots is their propulsion and steering. Here, swimming microorganisms could be useful due to their self-powered movement and controllable steering properties, based on biological propulsion and sensing. Magnetotactic bacteria (MTB) are microswimmers that align passively along the geomagnetic field and move actively toward their optimal environment using their flagella.[5] This so-called magnetotaxis depends on the biomineralization of magnetosomes, i.e., magnetic nanocrystals surrounded by a membrane. Typically, the magnetosomes are arranged in chains inside the cells, acting like a compass needle.[6]

Some researchers have employed bacteria as microrobots. One of the first reports demonstrated the controlled manipulation and actuation of micro-objects with MTB.[7] Later, manipulation of swimming properties were investigated.[8] Another group used magnetically guided MTB to separate pathogenic bacteria.[9] MTB were accumulated in tumor regions using aerotaxis and magnetotaxis by delivering them intravenously in mice.[10,11] However, in vivo medical applications of MTB and biocompatibility test with an active immune system have not been shown yet.[12] Moreover, MTB are difficult to cultivate in the laboratory, since they need microaerobic conditions and complex chemical gradients.[13] Another disadvantage is their reduced applicability as transporters: the velocity of MTB was reduced about 85% when loaded with a polystyrene bead.[14] Also, other fast swimming bacteria like *Serratia marcescens, Salmonella typhimurium,* or *Escherichia coli* were investigated for microrobotic applications.[2,15,16] But, these bacteria have certain limitations: they do not show magnetic behavior and could be pathogenic for animals and humans. In a

Dr. G. Santomauro, M. Mohammadrahimi, Prof. J. Bill
Institute for Materials Science
University of Stuttgart
70569 Stuttgart, Germany
E-mail: santomauro@imw.uni-stuttgart.de
Dr. A. V. Singh, Dr. P. Erkoc, Prof. M. Sitti
Physical Intelligence Department
Max Planck Institute for Intelligent Systems
70569 Stuttgart, Germany
Dr. B.-W. Park
Department of Civil/Environmental & Chemical Engineering
Youngstown State University
Youngstown, OH 44555, USA
Dr. E. Goering, Prof. G. Schütz
Modern Magnetic Systems Department
Max Planck Institute for Intelligent Systems
70569 Stuttgart, Germany
The ORCID identification number(s) for the author(s) of this article can be found under https://doi.org/10.1002/adbi.201800039.

**DOI: 10.1002/adbi.201800039**

 

recent study, such nonmagnetic bacteria could be also magnetically steered by attaching them to a magnetic robot body;[17] however, these bacteria-based swimmers can be still pathogenic.

In contrast, the nonpathogenic photosynthetic eukaryote *Chlamydomonas reinhardtii* microalga (spherical shaped, 5–10 µm in diameter) swims with the same velocity when loaded with a polymer bead (3 µm in diameter) as unloaded cells. Even, in microalgae with five or more attached beads, the velocity was only reduced to 50%.[18] These experiments were conducted in a microfluidic channel and the algae were steered by light. Photosynthetic microalgae need light for the production of energy, because of this, they swim toward the light (phototaxis) and can be steered by it. But *C. reinhardtii* shows also a forward motion in the dark,[19,20] which is crucial for the application inside the human body. In addition, it can be easily cultivated in the laboratory. Also, it has the capacity to carry a larger load, e.g., drugs, due to its larger body size.

Flagellar propulsion is considered to be an efficient and fast propulsion mechanism in a low Reynolds number hydrodynamic system like in small-diameter blood vessels, such as small arteriole, capillary sphincter, venule, and capillary vessels.[3,21] Both bacteria and eukaryotic microswimmers like *C. reinhardtii* use flagella for propulsion. In bacteria, a molecular motor rotates the helical flagella for forward propulsion using high viscous grad forces; in microalgae (as in all eukaryotes), the two flagella produce planar waves, such as breaststroke waves in *C. reinhardtii*, by bending.[3] The potential of using helical or planar wave-based microrobotic propulsion was compared by modeling.[22] It was found that the planar wave propulsion has a higher efficiency at 100% efficiency for the actuator. This makes the application of eukaryotic microswimmers as microrobots more attractive than MTB. But microalgae like *C. reinhardtii* lack magnetotactic behavior and can thus not be steered inside the human body, which is optically not transparent in deep regions.

In this work, we investigated a possible magnetotactic performance of the microalga species *C. reinhardtii*. First, we tested the magnetization potential of the microalgae by culturing them in media containing terbium ions ($Tb^{3+}$). The lanthanide Tb is selected here since it shows high magnetic properties,[23] even higher than iron. Another advantage of $Tb^{3+}$ is its photoluminescence and thus its applicability as a biomarker. Next, we tested the magnetotactic behavior of the $Tb^{3+}$ treated microalgae in a magnetic field. Additionally, we investigated the biocompatibility of *C. reinhardtii* microalgae with mammalian cells by co-culturing both cell types.

## 2. Results and Discussion

### 2.1. Culturing of *C. Reinhardtii* and Terbium Accumulation in the Cells

We incubated cells at pH 4.8 in BG (blue-green algae) 11 media containing 6.5 mg $L^{-1}$ $Tb^{3+}$, chelated equimolar with ethylenediaminetetraacetic acid (EDTA). Both the pH and the ligand were used to prevent precipitation of the $Tb^{3+}$ and thus to maximize its uptake.[24,25] Furthermore, with lower pH, the adsorption rate onto cell walls of microalgae is enhanced.[26] Adsorption on the cell wall is the first accumulation step of metal ions in microalgae. Additionally, lanthanide–EDTA complexes can alleviate lanthanide growth inhibition of microalgae.[27] Our cultures with added $Tb^{3+}$ showed a growth rate inhibition on the third day as well as on the seventh day of the experiment of about 50% compared with the reference (**Figure 1**). This is within the same range as described before for marine and freshwater microalgae.[27,28] At low concentrations (less than 4 mg $L^{-1}$), lanthanides have stimulatory effects on microalgae but can be toxic in high concentrations.[28,29] The mean speed of our microalgae was not affected by cultivating them with added $Tb^{3+}$ (see chapter 2.3.2. and Figure 5). The effect of $Tb^{3+}$ on the microalgae species *C. reinhardtii,* used in our study, was not described before.

Before chemical analyses via inductively coupled plasma optical emission spectrometry (ICP/OES), the cells were washed with diluted HCl solution to desorb adhering ions and to dissolve possible precipitates off the cell surface. In doing this, we investigated only ions accumulated inside the cells. A reculturing after this treatment revealed that the cells survived this washing procedure. We recorded that the average amount of incorporated $Tb^{3+}$ per cell was 0.23 ± 0.0027 picogram (pg). This uptake of $Tb^{3+}$ is possibly due to detoxification mechanisms of the cells toward the nonessential/toxic $Tb^{3+}$, as shown before for other positively charged ions like zinc or iron.[30–33] In general, the uptake of positively charged ions takes place in two steps: the first is a rapid passive biosorption onto the cell wall to negatively charged functional groups, followed by a slow, energy consuming membrane transport.[26,34] If the accumulated ions

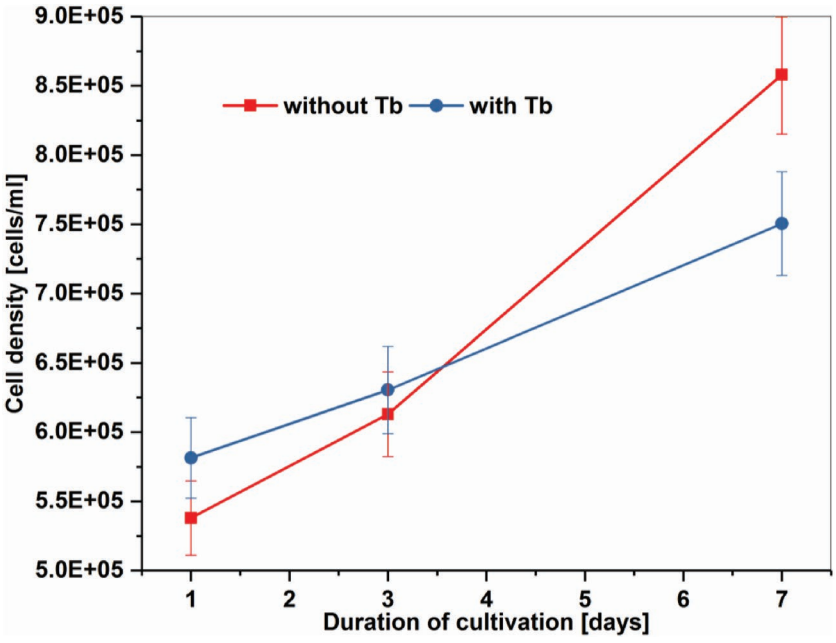


**Figure 1.** Proliferation of the experimental cultures containing 6.5 mg $L^{-1}$ $Tb^{3+}$ and the reference without $Tb^{3+}$. On day 1 the experiment started. Values shown are mean ± standard deviation of mean from three different experiments ($n$ = 3).

are toxic or inessential, the cytoplasm is detoxified afterward by chelating the ions to ligands thus making them nonreactive.[35] We could recently show that inessential zinc ions are incorporated into the coccoliths of the microalga *Emiliania huxleyi*[36] or mineralized to zinc–phosphate nanoneedles in the microalga *Scendesmus obliquus*.[30] Although lanthanides occur mostly as trivalent cations, their coordination properties are very similar to divalent metal ions like $Ca^{2+}$, $Mg^{2+}$, or $Fe^{2+}$ and can replace them in biomolecules.[37,38] The uptake of lanthanides like $Nd^{3+}$ or $Sm^{3+}$ by microalgae seems to be dependent on $Ca^{2+}$-channels in the cell membrane.[39,40]

In recent years, research on the reaction of algae toward different lanthanides increased. Mostly, their biological effect on growth and toxicity[27–29,41] or the biosorption onto the cell (wall)[24–26] was reported. Only few reports investigated the accumulation amount of lanthanides inside the cells. The transportation and accumulation of the lanthanide neodymium ($Nd^{3+}$) into *Euglena* cells was analyzed.[39] Culturing the cells for 3 d in $Nd^{3+}$ containing media yielded an amount of 2.0–2.9 pg $Nd^{3+}$ per cell. In this study with *C. reinhardtii* cells, it was shown to be 0.22–0.27 pg $Tb^{3+}$ per cell. The values for both algae species are comparable, since *Euglena* cells are ≈10 times larger than *C. reinhardtii*. Furthermore, the biological effect and the accumulation potential of different lanthanides and also for varying microalgae species are different.[28,29] The mechanism of incorporation or storage of lanthanides in microalgae is still not clearly understood.[41]

### 2.2. Photoluminescence Behavior

Lanthanides show photoluminescence, this means that they emit photons (light) of a characteristic wavelength resulting in a characteristic color of the element. This feature is also correct when incorporated in different materials, thus lanthanides are attractive probes for molecular sensing.[42,43] To receive luminescence of the materials, only trace amounts of the lanthanide are needed. $Tb^{3+}$ exhibits four specific emission wavelengths and shows green luminescence with a main peak at around 544 nm.[44,45]

We analyzed the photoluminescence of the $Tb^{3+}$ untreated and treated *C. reinhardtii* cells as reference and experimental samples, respectively. In order to confirm the position of the emitted luminescence light from the accumulated $Tb^{3+}$ inside the cell, we first washed the cells with diluted HCl solution to remove free $Tb^{3+}$ physically absorbed on the cell wall of the cell. Then the cells were drop casted and air-dried on a silicon wafer and investigated by a photometer. The sample exhibits specific $Tb^{3+}$ emission peaks, including the main green peak at 542 nm (**Figure 2**). The untreated *C. reinhardtii* cells did not show the characteristic $Tb^{3+}$ peaks (red curve). These photoluminescence results, correlated with the ICP/OES data, show that $Tb^{3+}$ were specifically accumulated inside the cell.

### 2.3. Magnetic Properties

#### *2.3.1. SQUID Measurements*

We performed a magnetization measurement with a Quantum Design MPMS3 VSM SQUID for the samples prepared after 7 d of culture in the growth media with and without $Tb^{3+}$. For the VSM measurement, the cell samples were placed into a quartz glass capsule, and measured at 100, 200, and 250 K. Diamagnetic background, from the capsule and the DI water, and superimposed paramagnetic background, for example from iron ions in the cells, were subtracted by an effective simple linear slope.

At 200 K, the paramagnetic response (Brillouin Function) from any magnetic ions as Fe or Tb solved in the water is almost perfectly linear with positive slope in the field range available in the SQUID (7T), also following a Curie $1/T$ law as a function of temperature.[46] In contrast, diamagnetism related to DI water and the sample containment, which is a pure quartz glass capsule, is almost temperature independent and perfectly linear for all available fields and temperatures, but with a negative slope. As a superposition the high field behavior of all SQUID M(H) measurements are linear and negative in slope, just showing the dominating diamagnetic background. As the paramagnetic background could not simply estimated and subtracted from a single M(H) loop, the total sum of both linear responses is subtracted by a linear fit applied at the high field regions for the M(H) loops. The slope in units of emu per Oe is

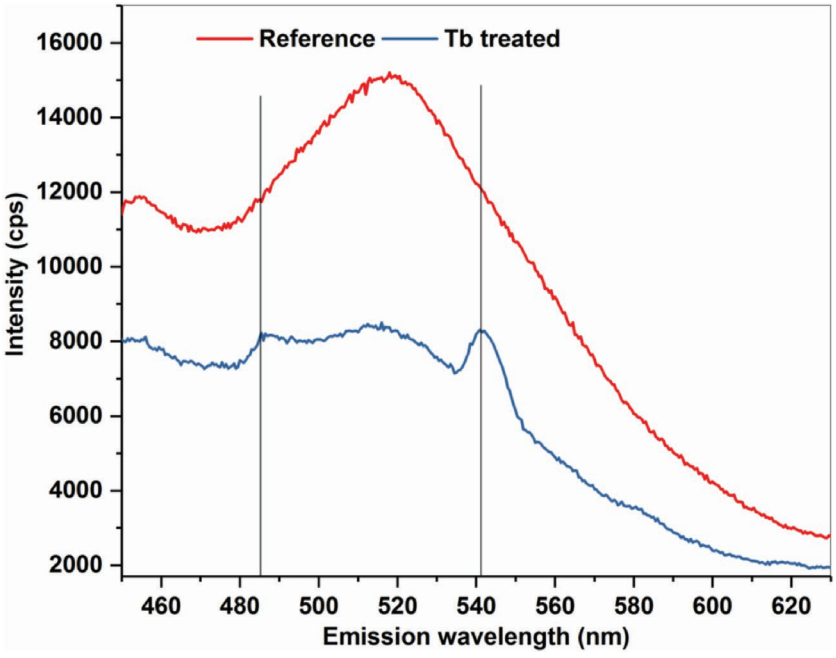


**Figure 2.** Photoluminescence of cells incubated for 7 d with $Tb^{3+}$. Reference was grown without $Tb^{3+}$. $Tb^{3+}$ specific emission peaks can be observed, indicating that $Tb^{3+}$ was taken up by the cells. The emission color of the whole sample is green, according to the main peak at 542 nm.

then multiplied by the measurement field and subtracted from the original data. As a result the shown M(H) curves do just provide the remaining superparamagnetic part of the signal provided by the algae.

The reference sample treated without $Tb^{3+}$ and the pure quartz glass capsule had almost the same superparamagnetic like background. Therefore, within the given error bar we cannot identify any superparamagnetic signal at the reference algae. The microalgae doped with $Tb^{3+}$ clearly showed a clear superparamagnetic signal half an order of magnitude higher than the reference sample (**Figure 3**). Therefore, the uptake of $Tb^{3+}$ inside the cells results in superparamagnetic properties. Consequently, we produced magnetic microswimmers by incorporation of $Tb^{3+}$.

Superparamagnetism means that the cells only show magnetic behavior when a magnetic field is applied, which is advantageous when they are used as microtransporters inside the human body. If remnant magnetization phenomena would be present, magnetic dipole interaction between the algae could result in unwanted agglomeration phenomena.

To calculate the magnetic moment of a single cell doped with $Tb^{3+}$, we normalized the magnetic moment measured by SQUID of the whole sample by the number of cells, which we counted before the SQUID analyses. Thereby, we calculated a magnetic moment of $1.6 \times 10^{-11}$ emu for one single $Tb^{3+}$ doped *C. reinhardtii* cell; that is comparable with its counterparts reported as magnetotactic microswimmers. For example, the magnetic dipole moment of rod-shaped, 5 µm long MTB is reported to be $3.7 \times 10^{-13}$ emu,[47] and that of spherical MTB with diameters of 4–5 µm is $1.4 \times 10^{-11}$ emu.[8,48] Even though the magnetic moments of the two microorganisms are comparable, *C. reinhardtii* have an ≈15 times larger body volume than spherical shaped MTB and it is a fast breaststroke swimmer with two powerful flagella, which might make magnetic steering of the microalgae more challenging than MTB.

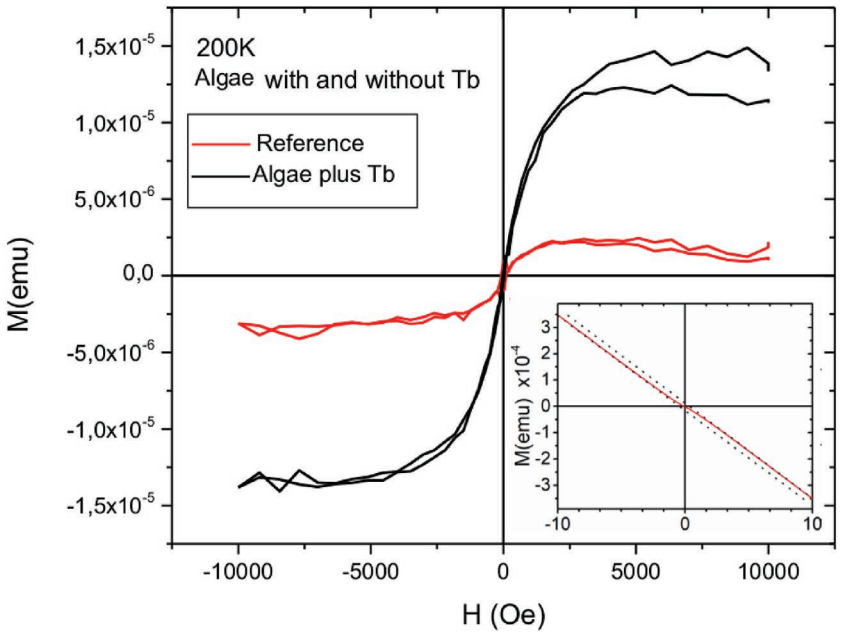


**Figure 3.** SQUID measurements at 200 K of cells treated for 7 d with $Tb^{3+}$ and reference grown in media without $Tb^{3+}$. Only the $Tb^{3+}$-doped cells show superparamagnetic behavior, the reference has the same magnetic signal like the empty glass capsule. This indicates that the intracellular accumulation of $Tb^{3+}$ caused superparamagnetic properties of the *C. reinhardtii* cells. The inset shows raw data of the $Tb^{3+}$-enriched algae sample, including the linear fit, where the slope has been used to subtract the dia- and paramagnetic background. For details, see text.

### 2.3.2. Steering of the Magnetized Microswimmers

We carried out magnetic guiding, that is, the directional motion of the magnetized microswimmers using a permanent magnet-based uniform magnetic field generation setup (**Figure 4**).[49,50] The uniform magnetic field was generated in the ROI region without magnetic gradient. The swimming directions of the algae cells were observed in the dark, avoiding phototactic orientation.[19] The swimming motions of the untreated and the magnetized cells under the magnetic field were analyzed to evaluate the directionality of the motion. We quantified the swimming direction based on the 2D distribution of the swimming biased along the magnetic field. The heading direction was obtained by analyzing segments moving along x-axis. The distributions of the swimming heading were obtained by analyzing the number of frames of the orientation angle within a defined angle interval.[49] The magnetic field strength was found to be 161.3 mT with a Gauss meter and the uniform magnetic field without a gradient was obtained.

The strong permanent magnet-based setup was selected for three reasons: 1) Unlike an electromagnetic coils-based setup, permanent magnets do not generate heat, which is necessary to avoid a temperature-induced influence on the behavior of the biohybrid microswimmers (20–32 °C optimum for *C. reinhardtii*).[20] 2) The microalgae containing a small amount of $Tb^{3+}$ could only be controlled by a strong magnetic field. 3) By applying two parallel magnets, we generated a magnetic field with corresponding lines, where the magnetized cells can align on and subsequently swim toward one magnet and are not only attracted by the magnet. We analyzed the trajectories of the untreated microalgae under the magnetic field (11 videos, $n = 42$) and the magnetized microswimmers under magnetic field (10 videos, $n = 26$) that displayed a random motion and a biased motion parallel to the direction of the applied field, respectively, as shown in Figure 4D,E (Videos S1 and S2, Supporting Information). For untreated algae, the angular distribution of the swimming heading is isotropic, and the 2D mean speed was measured to be $23.4 \pm 4.5$ µm $s^{-1}$. Whereas the $Tb^{3+}$-treated magnetized microswimmers were shown to have a biased swimming motion along the magnetic field

direction demonstrating anisotropic magnetotactic behavior and the mean speed of 21.7 ± 7.1 μm $s^{-1}$. In addition, the mean speeds of untreated (10 videos, $n$ = 39) and magnetized microswimmers (10 videos, $n$ = 46) without magnetic field were found to be 23.8 ± 5.1 and 22.9 ± 4.4 μm $s^{-1}$, respectively. The only slight differences of the mean speeds between these three types of microswimmers, the $Tb^{3+}$-treated cells without magnetic field, the untreated reference without and that with magnetic field, suggests that the mean speed reduction of the $Tb^{3+}$-treated cells in the magnetic field is not due to any influence of $Tb^{3+}$ (**Figure 5**). The mean speed reduction (about 7%) of the magnetized cells in the magnetic field may be attributed to the influence of the magnetic field aligned to the parallel to the swimming direction and the alignment of the cells onto these field lines,[49] which may have a negative effect on the swimming speed of the algae.

### 2.4. Choice for $Tb^{3+}$ as the Magnetizer

We used wild type *C. reinhardtii* cells for the facile magnetization via incorporation of $Tb^{3+}$ unlike magnetosome biogenesis which require genetic engineering.[50] The advantage of using $Tb^{3+}$ as the magnetizer lies in its photoluminescence property and thus the applicability as a marker.[42,37] $Tb^{3+}$ can be easily detected even in trace amounts and represents a very sensitive fluorescent tracer. Since green algae intrinsically emit fluorescence due to, e.g., chlorophyll and additionally

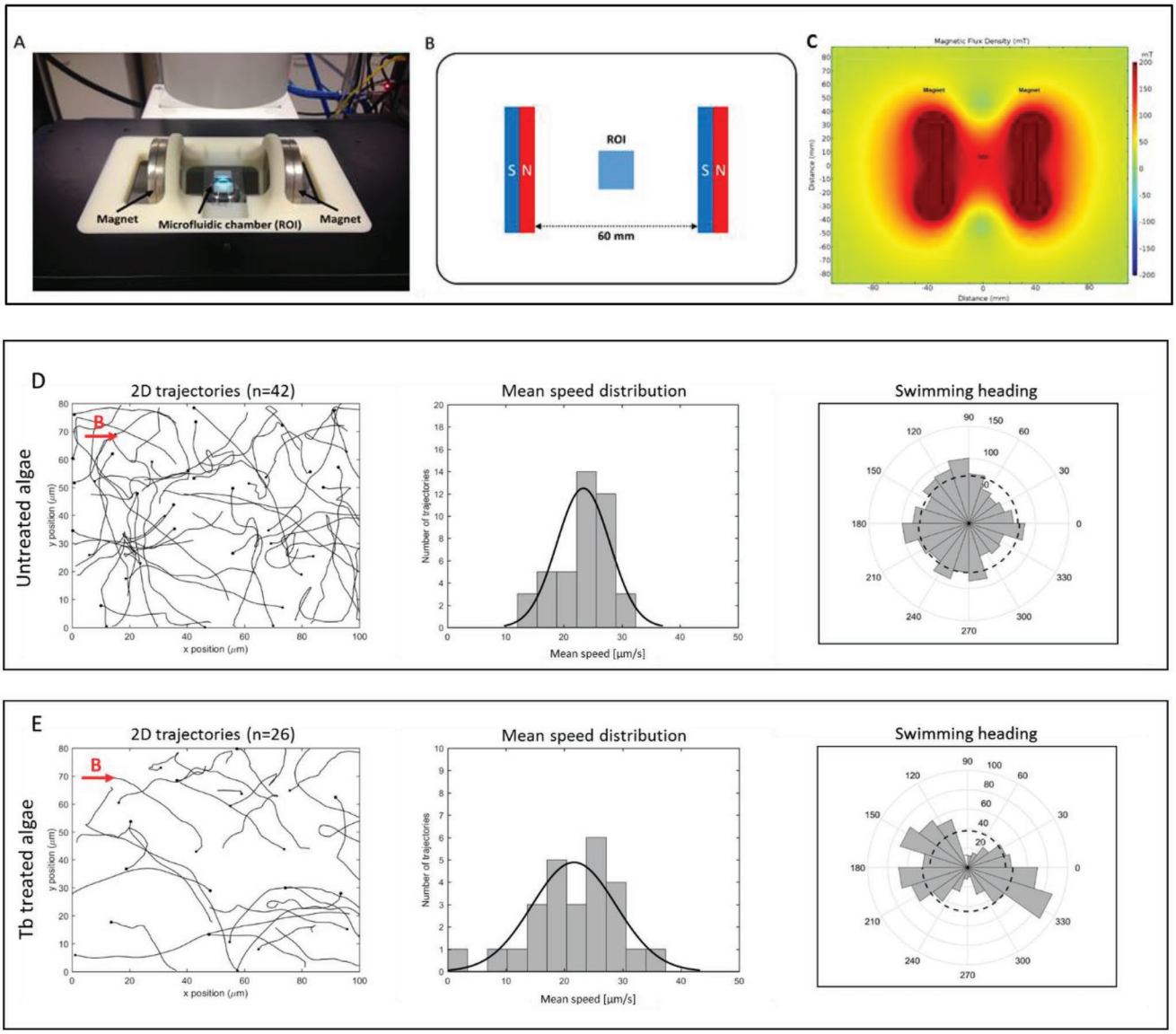


**Figure 4.** A) Magnetic guidance setup with the microfluidic chamber, the region of interest (ROI) between two permanent magnets. B) Schematic representation of the magnetic setup. C) COMSOL simulation diagram of the magnetic field. D,E) 2D trajectories, mean speed distribution fitted by a normal distribution curve, and swimming heading of the untreated microalgae and the magnetized microswimmers. $Tb^{3+}$-treated cells show directional motion parallel to the direction of the applied uniform magnetic field (161.3 mT) using two magnets separated by a distance of 60 mm. 11 videos ($n$ = 42 cells) of untreated microalgae and 10 videos ($n$ = 26 cells) of magnetic microswimmers were analyzed.

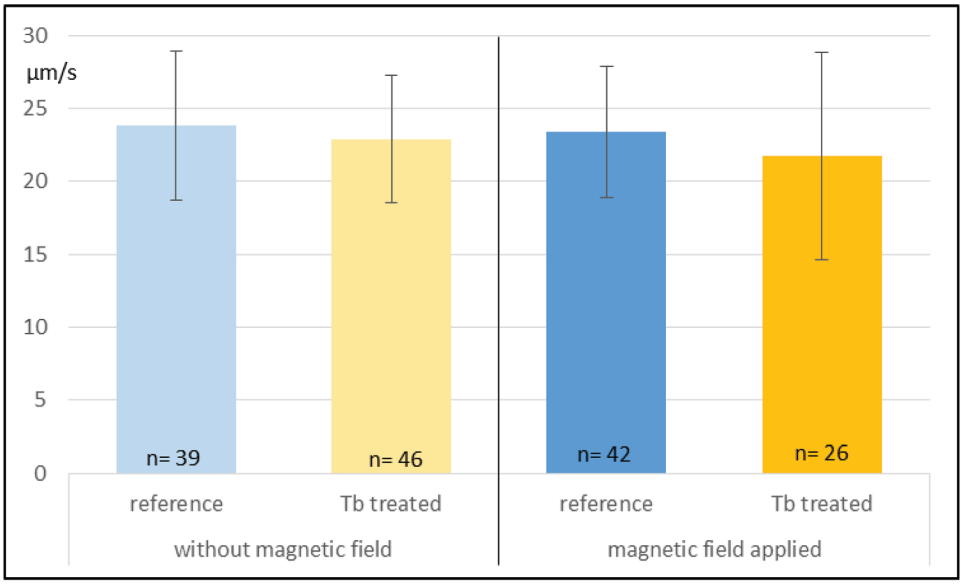


**Figure 5.** Mean speed of untreated and Tb-treated cells without and with magnetic field applied, respectively.

gained luminescence properties by $Tb^{3+}$ treatment, they can be more easily tracked inside the human body, e.g., in the eye. The non-toxic lanthanides were used before as indigestible markers and inert tools for evaluating diet ingestion in animal and human nutrition.[51,52] When microrobots are applied as drug delivery systems, they have to be considered of being removed from the human body. Non-pathogenic *C. reinhardtii* cells can be digested or degraded in the human body and the residues can leave the body through natural excretory pathways. Though the fluorescent $Tb^{3+}$-containing remainders may not be digested, their fate can be tracked by analyzing excreted products such as the feces or the urine. In addition, $Tb^{3+}$ was reported to enhance the cytotoxicity of an anticancer drug.[53]

### 2.5. Biocompatibility of $Tb^{3+}$-Doped Algae for Biohybrid Microrobotics

Biohybrid microrobots have two components: a synthetic carrier and a biological actuator for propulsion.[54] It is important to assure the biocompatibility of both components: the synthetic part as a carrier should be made of biocompatible and biodegradable materials. Biological actuators, in this case the microalgae, should also be compatible with in vivo and in vitro conditions. Biological cells (e.g., bacteria, microalgae, mammalian cells) used as microrobotic actuators should not be pathogenic or not create any immunological issues.[55] In this context, bacteria have been extensively studied as propellers cooperated with attached drug carriers;[54] however, concerns remain regarding pathogenicity, and the easy genetic modification of their genome, which makes bacterial infection prone for such applications. To investigate the cytotoxicity of the eukaryotic microalga *C. reinhardtii*, we studied biocompatibility of the alga cells with a human breast cancer cell line and NIH 3T3 mouse fibroblast. We incubated the algae overnight with breast cancer cell line MCF-7 and NIH 3T3 mouse fibroblasts and captured overnight time-lapse videos. Video analysis show that the algae do not influence the motility and phenotype of MCF-7 and NIH 3T3 fibroblasts (**Figure 6**, Videos S3–S8 in Supporting Information), in addition, the alga and MCF-7/NIH 3T3 fibroblast cells still move, indicating mutual biocompatibility of both cell types. MCF-7 and NIH 3T3 cell overnight coculture with *C. reinhardtii* were shown in videos S3-5 and S6-8 (Supporting Information), respectively. Figure 6A–C demonstrates an overlay image taken after overnight coculture of MCF-7 cell monolayer (gray) with different seeding density of autofluorescence microalgae (red). The image exhibits normal cell phenotype of both cell types. To evaluate MCF-7 cell viability, cell proliferation and live/dead cell assays were carried out. As shown in Figure 6D, cell proliferation in the microalgae treated cells shows a similar proliferation profile like routine cell culture and we did not observed a significant change in cell proliferation index (t-test control vs high density *C. reinhardtii* = 0.13, $p \leq 0.05$). In addition, percentage of live cells in microalgae-treated samples was shown to be similar to untreated MCF-7 cells culture, indicating non-cytotoxic nature of *C. reinhardtii*.

Next, we looked morphological and cytoskeleton changes in MCF-7 cells if any induced by microalgae-loaded samples using confocal imaging. As show in Figure 6F–G, actin organization is well preserved with bundled and straight actin filaments in microalgae treated samples similar to the control MCF-7 cells. In the previous in vitro model, in spite of preserved cytoskeleton, cell organelles like mitochondria are known to be influenced by the presence of microswimmers.[56] Mitochondria are well known to be influenced by minor changes into cells environment in response to oxidative stress.[57,58] In this context, we immunostained mitochondria along with the cytoskeleton, but pattern and dye uptake by healthy mitochondrial compartment demonstrate qualitatively similar appearance (Figure 6F,G). 3D buildup obtained with the confocal laser scanning microscopy in *z*-direction (14 slices each 0.5 µm thick, video S9, Supporting Information) and 360° turn around in y-axis (in screen space; (video S10, Supporting Information) of stacked

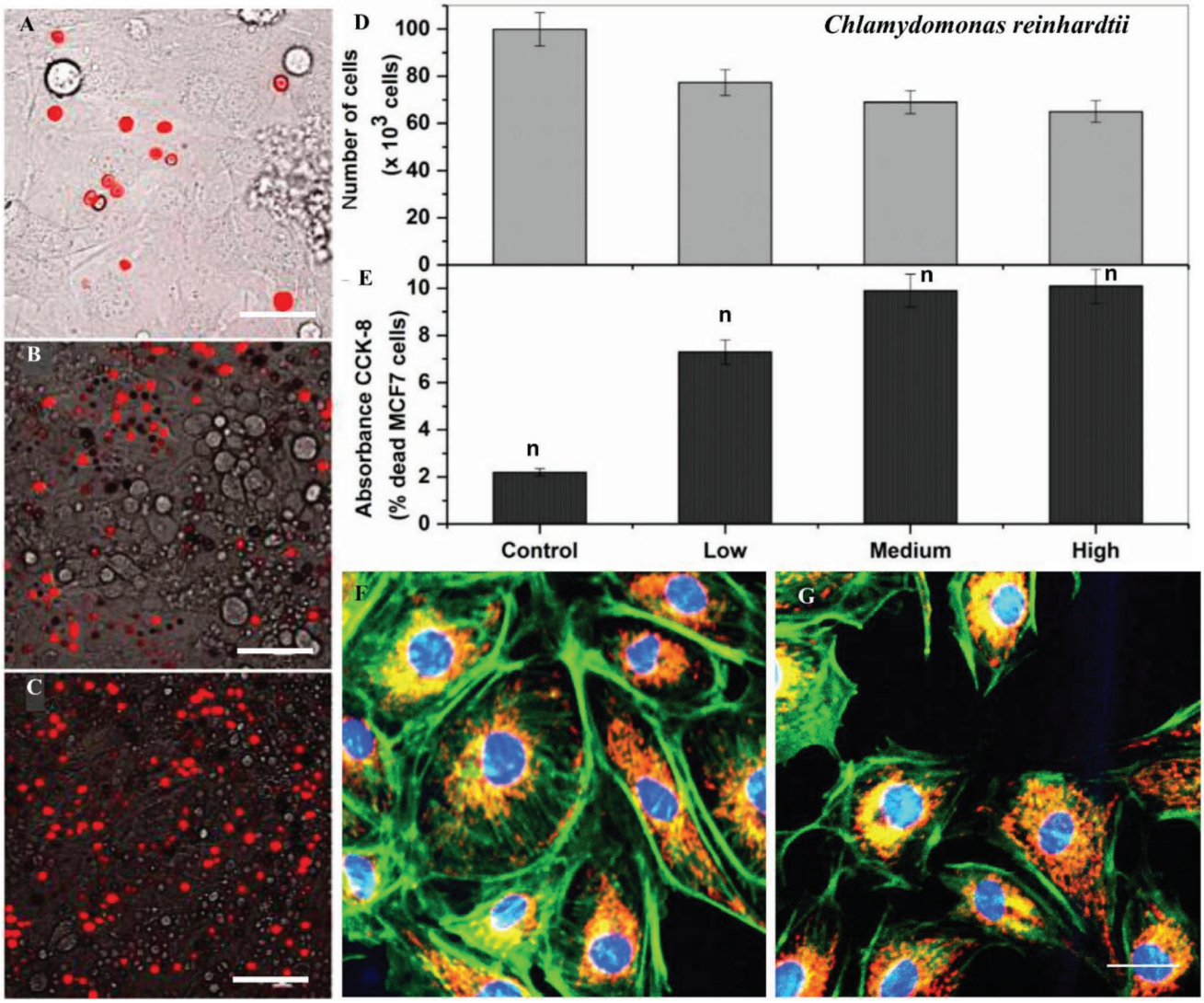


**Figure 6.** Biocompatibility of breast cancer MCF-7 cells in an overnight co-culture with *C. reinhardtii* cells. A–C) Three different microalgae concentrations (A-Low, B-medium, C-high) were added to cancer cells as shown in the overlay. D,E) Cell proliferation and live dead assay for quantitative analysis of cell functions. Values shown are mean ± SEM from five different experiments performed in triplicate ($n = 5$; t-test control vs high density *C. reinhardtii* = 0.13, $p \leq 0.05$; n indicates nonsignificant). Cytoskeleton and mitochondrial staining to assess stress response. F) Control MCF-7 cells (untreated) showing microactin bundles (green) and mitochondria (red) with counterstained nuclei (blue DAPI). G) Co-culture of MCF-7 and *C. reinhardtii* cells showing similar staining like control cells (scale bar: 50 µm).

actin-mitochondria and nuclei stained images as stacks demonstrate much clear view of cytoskeleton and mitochondria inside MCF-7 cells. These results clearly indicate that *C. reinhardtii* is a biocompatible candidate for future microrobots towards medical applications.

## 3. Conclusion

In this study, we present a proof-of-concept that by incorporation of terbium into a microalga magnetotactic behavior can be achieved. In addition to the steering of innately photosensitive *C. reinhardtii* based on phototactic guidance reported previously,[20] here we wanted to control the movement of the microswimmers by magnetization. For this purpose, we incubated the microalgae in terbium ($Tb^{3+}$)-enriched media. The cultures showed a growth rate inhibition, but the swimming speed of the cells was not affected by the $Tb^{3+}$ treatment. The internalization of $Tb^{3+}$ was confirmed via chemical and fluorescence intensity characterizations.

SQUID measurements revealed the superparamagnetic like properties of the $Tb^{3+}$-doped microalgae. The $Tb^{3+}$-treated cells revealed a five times higher magnetization than the reference sample or the pure quartz container capsule. One single $Tb^{3+}$ doped *C. reinhardtii* cell showed a magnetic dipole moment of $1.6 \times 10^{-11}$ emu, which is comparable to the magnetic moment of magnetotactic bacteria.

The magnetized *C. reinhardtii* cells could be magnetically guided in the dark by applying a strong magnetic field, which induces a torque. Along the magnetic field lines the

magnetized microalgae passively aligned, and subsequently swam in a single direction toward one magnet. Thus, our swimming directory results present the generation of terbium-based magnetized microalgae showing magnetotactic behavior like magnetotactic bacteria, i.e., align passively to magnetic field lines and swim actively towards a magnet.[59]

Moreover, we investigated the biocompatibility of *C. reinhardtii* cells on human breast cancer cells (MCF-7) and mouse fibroblasts (NIH3T3) as a healthy cell control. Mammalian cell viability and proliferation were characterized by means of the motility, phenotype, and morphology after overnight incubation with microalgae. The results indicate that the microalgae are nontoxic/nonpathogenic, and seem biocompatible to tested cell lines. *C. reinhardtii* cells were still able to swim during the co-culture, indicating mutual biocompatibility of both the cell types.

In conclusion, our study demonstrates the generation of a fast swimming, bio-hybrid magnetotactic microswimmer by uptake of $Tb^{3+}$ ions into the living algae cells. Incorporation of $Tb^{3+}$ as the magnetizer into the system also provide an additional benefit, the trackability due to the photoluminescence of the lanthanide. Moreover, we showed biocompatibility of microalgae on mammalian cells and viability of these microorganisms in mammalian cell culture conditions. These microswimmers can be considered for biomedical applications as they offer accurate guidance systems. Moreover, they can be loaded with drugs,[60] modified by nano/microcarriers[18,61] imaging agents[62] and engineered to carry therapeutic genes.[63] Magnetized *C. reinhardtii* cells could be utilized in future drug delivery and/or drug screening approaches for potential cancer treatments.

## 4. Experimental Section

*Organisms and Cell Cultures*: All glass vials were rinsed in 0.02 M hydrochloric acid for 24 h before use to remove adherent molecules. The experiments were conducted with living *C. reinhardtii* (strain 11-32), obtained from the SAG culture collection Göttingen. The algae were cultivated in BG 11 medium at room temperature and under a 12:12 light-dark cycle (Philips MASTER TL-D 58W/840 Super 80 Weiss) in 250 mL Erlenmeyer flasks, sealed with a permeable membrane to prevent contamination but allow ventilation. The experimental medium was prepared by adding 6.5 mg $L^{-1}$ $Tb^{3+}$, chelated equimolar with EDTA (all chemicals Sigma). This ligand was used to prevent precipitation of terbium complexes and thus to enhance its bio-uptake.[25] The references were cultivated without $Tb^{3+}$. All cultures including the references were adjusted to pH 4.8 each day, since at this pH lanthanides exist as $Ln^{3+}$ and thus can be taken up by the microalgae.[24] On the first day, when the experiment started, the third and the seventh day, the number of cells was counted with a hemocytometer (Marienfeld, Lauda-Königshofen) to investigate the development of the cultures. The duration of the experiments was 7 d.

*Chemical Analyses of $tb^{3+}$ Inside the Cells*: After 7 d culturing at pH 4.8, the amount of $Tb^{3+}$ in the cells was analyzed via ICP-OES (Spectro CIROS). In two identical experiments, 4 and 5 mL culture incubated with $Tb^{3+}$ were analyzed. The reference was 6 mL of a culture incubated at pH 4.8 without added $Tb^{3+}$. The algae were first washed five times with deionized water (Millipore) to remove the medium and unattached molecules. Afterward, the cells were washed in hydrochloric acid (0.02 M, pH 3) for 30 min on a rotary shaker to dissolve the possibly attached ions and again washed with deionized water (DI) to remove the acid. Desorption experiments using a brown alga have shown that removing of lanthanides with diluted HCl is successful.[24] Reculturing after wash revealed that the cells survived this treatment. SEM pictures showed that no precipitation was associated with the cells afterward. Using this washing procedure, only $Tb^{3+}$ inside the cells was recorded. After the washing step, the number of cells was counted using a hemocytometer. Then the cells were dried at room temperature, digested in concentrated $H_2SO_4/HNO_3$ (nitric acid), mineralized at 250 °C and finally suspended in deionized water (Millipore). This solution was analyzed via ICP-OES to detect $Tb^{3+}$ inside the cells.

*Photoluminescence Investigations*: Photoluminescence (PL) properties of the cells treated for 7 d with $Tb^{3+}$ were analyzed via PL spectroscopy (FluoroLog, Horiba Yobin Yvon). The cells were prepared as described in chapter "chemical analyses." After the last washing step with deionized water, $9 \times 10^5$ cells were dropped onto a silicon wafer (cleaned with ethanol) and dried at room temperature. The PL of $Tb^{3+}$-treated cells and untreated reference were observed after excitation at a wavelength of 300 nm appropriate for the specific $Tb^{3+}$ emission spectrum.[45]

*SQUID Measurement*: To measure the magnetic moment of the *C. reinhardtii* cells incubated with $Tb^{3+}$, commercial Quantum Design MPMS3 SQUID (Superconducting Quantum Interference Device) system was used. The sample preparation was as described in chapter "chemical analyses." After counting the washed cells, they were interacting for enrichment purposes with an NdFeB permanent magnet overnight. Afterward, they were pipetted into a glass capsule (cleaned with HCl) and frozen at 200 K. The magnetization behavior of the cells incubated for 7 d in $Tb^{3+}$ containing medium as well as the reference without $Tb^{3+}$ was measured at 100, 200, and 250 K. A cleaned quartz glass capsule filled with DI water was measured as base line.

*Evaluation of the Steering Properties of Magnetized C. Reinhardtii Cells*: Magnetic steering properties and mean speed measurement of *C. reinhardti* cells were studied on a customized set in our laboratory (schematic Figure 4)[49] after overnight interaction for enrichment purposes with an NdFeB permanent magnet. Directional motion of the magnetized microswimmers and the untreated reference was examined using an one-directional magnetic guidance setup consisting of two disc-shaped permanent magnets separated by a distance of 60 mm, axially magnetized, and 60 mm in diameter (NdFeB, N42, Webcraft GmbH, Germany). A custom-made microscope stage surrounding a PDMS microfluidic chamber (thickness = 300 µm) was placed onto a Zeiss Axio Observer A1 inverted microscope with an Axiocam 503 CCD camera and a 40× (NA = 0.6) objective lens. This setup is suitable for generating a uniform magnetic field in the region of interest (ROI), so that the microswimmers can orient along one direction.[37] The algae were illuminated using a red filter with emission peak at 655 nm and a band width of 15 nm (655/15 BrightLine HC, AHF Analysentechnik, Tübingen, Germany), avoiding phototactic orientation of the cells.[19] Magnetized *C. reinhardtii* cells (10 videos, $n = 26$) and untreated algae (11 videos, $n = 42$) were exposed to a uniform magnetic field at 161.3 mT and their 2D (xy-dimension) swimming trajectories and speed were recorded and analyzed using an in-house tracking program developed in MATLAB R2015a (Mathworks, Natick, USA). The details of this algorithm are described in our previous publications.[37,49] The magnetic field in the ROI was measured with a Lake Shore Cryotronics (Darmstadt, Germany) model 460 three-channel Gauss meter. Additionally, the swimming speed of magnetized *C. reinhardtii* cells (10 videos, $n = 46$) and untreated algae (10 videos, $n = 39$) were measured without magnetic field (Figure 5).

*Cell Proliferation and Cytotoxicity Assay*: For all biocompatibility tests Human breast cancer cells (MCF-7), provided by American Type Culture Collection (ATCC HTB-22) and NIH 3T3 mouse fibroblast (ATCC CRL-1658) were used. MCF-7 and NIH 3T3 was seeded in ibidi 8 chambered microwells with glass bottom at a seeding density of $5 \times 10^4$ cells $mL^{-1}$ in complete low glucose DMEM (Life technologies, Germany) and grown for 3 d (70% confluency, $\approx 10^6$ cells per well) at 37 °C in a humidified incubator containing 5% $CO_2$. Overnight culture of MCF-7 or NIH 3T3 was established in a 96-well plate. $Tb^{3+}$ doped *C. reinhardtii* cells in sterile BG 11 media were directly added to the MCF-7 monolayer. After incubation the cells were washed thoroughly with sterile PBS (1×) to wash away algae from MCF-7 cells monolayer. MCF-7 cells were

observed under microscope to make sure that the majority of algal cells were washed away, however, it is difficult to wash 100% of the algae from MCF-7 cell surface. Out of 10–15 algal cells can be seen over the MCF-7 surface. Biocompatibility was assayed with the cell counting Kit-8 (cat # CK04-20, tebu-bio), which is a colorimetric assay for the determination of viable cell numbers and can be used for cell proliferation assays as well as cytotoxicity assays. Cell Counting Kit-8 uses a tetrazolium salt, WST-8, which produces the water-soluble WST-8 formazan. Since this orange colored formazan does not require dissolving, no solubilizing process is required. Results were obtained after three simple steps: by 1) adding 10 µL of CCK-8 solution to each well of the 96 plate, 2) incubating the plate for 1–4 h in the incubator, and 3) measuring the absorbance at 450 nm using a microplate reader. WST-8 is not cell permeable, which results in low cytotoxicity.

*Viability of C. Reinhardtii Incubated with MCF-7 or NIH 3T3 Cells*: The sample from the reactor was stained using $10 \times 10^{-6}$ M SYTOX Green (Molecular Probes, USA) in TAP media for 10 min at room temperature. Live cells in the sample were observed at 488 nm (Ar-laser)/505–530 nm (excitation/emission) and dead cells were observed at 543 nm (HeNe-laser)/560 nm (excitation/emission) using a confocal laser microscope (LSM 510 META, Carl Zeiss, Germany). The ZEN 2009 Light Edition software (Carl Zeiss, Germany) was used to merge dual fluorescence images. About 500 cells in a random field at 100 × magnification was utilized to calculate the cell death of *C. reinhardtii*.

*Cell Culture and Time-Lapse Video Microscopy*: MCF-7 cells at seeding density of $5 \times 10^4$ cells mL$^{-1}$ were allowed to attach and make a confluent monolayer in high magnification microscopy compatible glass bottom microwells (Ibidi, Germany) in DMEM media supplemented with 10% FBS (Gibco, Germany) and antibiotic (Penicillin/streptomycin, Sigma). The dishes were placed on TCS-SP2 AOBS (Leica) at 20× with proper phase contrast filters and equipped with the incubation chamber (H301-EC-BL, Okolab) to keep the cells at 37 °C. Just before recording time lapse videos, cell monolayer was washed and fresh harvested *C. reinhardtii* at low ($1 \times 10^3$), medium ($2.5 \times 10^3$), and high ($5 \times 10^3$ cells mL$^{-1}$) concentration were added to the MCF-7 monolayer. Bright-field phase contrast images were collected every 5 min for overnight by a CoolSNAP HQ$^2$ CCD camera (Photometrics, AZ) connected to the Nikon Eclipse Ti Confocal Microscope with Yokogawa CSU-W1 spinning disk. Observed areas were randomly chosen for the time-lapse acquisitions from the entire population.

*Immunostaining Actin Cytoskeleton and Mitochondria*: Confluent culture of breast cancer cell line MCF-7 was seeded with high density microalgae and incubated at 37 °C for overnight. The cells were fixed with 4% paraformaldehyde (Sigma) for 30 min and washed with TBS, permeabilized with 0.5% Triton X-100 (Aldrich) for 10 min. The fixed cells were incubated in cytoskeletal buffer ($10 \times 10^{-3}$ M MES, $138 \times 10^{-3}$ M KCl, $3 \times 10^{-3}$ M $MgCl_2$, $2 \times 10^{-3}$ M EGTA, and 0.32 M sucrose) for 30 min.[51] For cytoskeleton (actin) double staining, the cells were incubated with phalloidin–FITC (1:400; Invitrogen) and mitotracker dye at $100 \times 10^{-6}$ M concentration (Life technologies) for 1 h. The samples were counterstained for nucleus (DAPI), fixed, and viewed at 63× magnification.

*Proliferation of the C. Reinhardtii Cultures and Chemical Analysis of $Tb^{3+}$*: *Statistical Analysis*: The proliferation of three cultures with and three cultures without added $Tb^{3+}$ were investigated. The number of cells on the first day, when the experiment started, the third day and the seventh day was counted using a hemocytometer with a pattern of 16 squares. The cells in each square were counted twice. For the evaluation of the mean values and the standard deviation, MICROSOFT EXCEL (2013) was used.

For the chemical analysis of the $Tb^{3+}$ inside the cells, in two identical experiments, 4 mL and 5 mL culture incubated with $Tb^{3+}$ were analyzed. The reference was 6 mL of a culture incubated without $Tb^{3+}$. The number of cells was counted using a hemocytometer with a pattern of 16 squares. The cells in each square were counted twice. For the calculation of the mean value and the standard deviation of incorporated $Tb^{3+}$ per cell, Microsoft Excel (2013) was used.

*SQUID Measurements*: A Quantum Design MPMS3 VSM SQUID was used for magnetization measurements. Diamagnetic background, from the capsule and the DI water, and superimposed paramagnetic background were subtracted by an effective simple linear slope. In order to see the $Tb^{3+}$ effect, a comparable amount of algae with and without $Tb^{3+}$ treatment was used. Before SQUID analyses, the exact amount of algae was determined by counting the cells of the $Tb^{3+}$-treated sample and the reference. To calculate the magnetic moment of a single cell doped with $Tb^{3+}$, the magnetic moment measured is normalized by SQUID of the whole sample by the number of cells.

For the SQUID data, no pre-processing has been applied, except the already described proportional removal of the para- and diamagnetic background.

*Steering and Swimming Speed Evaluations*: For the 2D trajectory data in a magnetic field, 11 videos ($n = 42$) of untreated microalgae and 10 videos ($n = 26$) of magnetic microswimmers were compared. For the swimming speeds without magnetic field, 10 videos ($n = 46$) of magnetized cells and 10 videos ($n = 39$) of untreated algae were compared.

The reported values of 2D motility analyses of the samples and assays were the averages of replicate experiments and were compared using one-way ANOVA followed by post hoc Tukey's multiple comparison test. The statistical analysis was performed using the softwares MATLAB R2017a (Mathworks, Natick, USA) and OriginPro 2016 (OriginLab, Northampton, USA). The differences were considered significant for $p$ value <0.05.

*Biocompatibility Testing*: For the biocompatibility tests, data were presented by the mean value with the standard error of the mean (SEM) as per commonly used protocols. Statistical analysis was performed using an unpaired or a paired t-test, two-tailed Student's t-test. $p$-value of <0.05 was considered to be statistically significant.

## Supporting Information

Supporting Information is available from the Wiley Online Library or from the author.

## Acknowledgements

The authors are grateful for financial support provided by the Deutsche Forschungsgemeinschaft (DFG) to G. Sa. The authors thank Samir Hammoud and Cem Balda Dayan from the Max Planck Institute for Intelligent Systems, Stuttgart for ICP-OES analysis and helps in simulation, respectively. The authors also thank Afarin Ershad from the University of Stuttgart for culturing of the algae.

## Conflict of Interest

The authors declare no conflict of interest.

## Keywords

magnetotactic swimmers, microalgae, microrobots, photoluminescence, terbium

Received: January 26, 2018
Revised: August 30, 2018
Published online:

[1] M. Sitti, *Mobile Microrobotics*, The MIT Press, Cambridge, MA **2017**.
[2] A. V. Singh, M. Sitti, *Adv. Healthcare Mater.* **2016**, *5*, 2325.
[3] B. J. Nelson, I. K. Kaliakatsos, J. J. Abbott, *Annu. Rev. Biomed. Eng.* **2010**, *12*, 55.
[4] A. V. Singh, Z. Hosseinidoust, B.-W. Park, O. Yasa, M. Sitti, *ACS Nano* **2017**, *11*, 9759.

 

[5] D. A. Bazylinski, T. J. Williams, C. T. Lefevre, R. J. Berg, C. L. Zhang, S. S. Bowser, A. J. Dean, T. J. Beveridge, *Int. J. Syst. Evol. Microbiol.* **2013**, *63*, 801.
[6] D. A. Bazylinski, R. B. Frankel, *Nat. Rev. Microbiol.* **2004**, *2*, 217.
[7] S. Martel, C. C. Tremblay, S. Ngakeng, G. Langlois, *Appl. Phys. Lett.* **2006**, *89*, 233904.
[8] S. Martel, M. Mohammadi, O. Felfoul, Z. Lu, P. Pouponneau, *Int. J. Rob. Res.* **2009**, *28*, 571.
[9] C.-Y. Chen, C.-F. Chen, Y. Yi, L.-J. Chen, L.-F. Wu, T. Song, *Biomed. Microdevices* **2014**, *16*, 761.
[10] M. R. Benoit, D. Mayer, Y. Barak, I. Y. Chen, W. Hu, Z. Cheng, S. X. Wang, D. M. Spielman, S. S. Gambhir, A. Matin, *Clin. Cancer Res.* **2009**, *15*, 5170.
[11] S. Martel, M. Mohammadi, *Micromachines* **2016**, *7*, 97.
[12] A. S. Mathuriya, K. Yadav, B. D. Kaushik, *Geomicrobiol. J.* **2015**, *32*, 780.
[13] C. T. Lefevre, A. Bernadac, K. Yu-Zhang, N. Pradel, L.-F. Wu, *Environ. Microbiol.* **2009**, *11*, 1646.
[14] Q. Ma, C. Chen, S. Wei, C. Chen, L.-F. Wu, T. Song, *Biomicrofluidics* **2012**, *6*, 24107.
[15] S. J. Park, S.-H. Park, S. Cho, D.-M. Kim, Y. Lee, S. Y. Ko, Y. Hong, H. E. Choy, J.-J. Min, J.-O. Park, S. Park, *Sci. Rep.* **2013**, *3*, 3394.
[16] S. J. Park, S. Cho, Y. J. Choi, H.-E. Jung, S. Zheng, S. Y. Ko, J.-O. Park, S. Park in *5th IEEE RAS & EMBS Int. Conf. on Biomedical Robotics and Biomechatronics (BioRob)*, IEEE, São Paulo, Brazil **2014**, pp. 856–860.
[17] R. W. Carlsen, M. R. Edwards, J. Zhuang, C. Pacoret, M. Sitti, *Lab Chip* **2014**, *14*, 3850.
[18] D. B. Weibel, P. Garstecki, D. Ryan, W. R. DiLuzio, M. Mayer, J. E. Seto, G. M. Whitesides, *Proc. Natl. Acad. Sci. USA* **2005**, *102*, 11963.
[19] M. Polin, I. Tuval, K. Drescher, J. P. Gollub, R. E. Goldstein, *Science* **2009**, *325*, 487.
[20] S. Xie, N. Jiao, S. Tung, L. Liu, *Biomed. Microdevices* **2016**, *18*, 47.
[21] D. de Lanauze, O. Felfoul, J.-P. Turcot, M. Mohammadi, S. Martel, *Int. J. Rob. Res.* **2014**, *33*, 359.
[22] K. C. Leptos, K. Y. Wan, M. Polin, I. Tuval, A. I. Pesci, R. E. Goldstein, *Phys. Rev. Lett.* **2013**, *111*, 158101.
[23] W. C. Thoburn, S. Legvold, F. H. Spedding, *Phys. Rev.* **1958**, *112*, 56.
[24] K. Vijayaraghavan, M. Sathishkumar, R. Balasubramanian, *Ind. Eng. Chem. Res.* **2010**, *49*, 4405.
[25] G. Yang, Q.-G. Tan, L. Zhu, K. J. Wilkinson, *Environ. Toxicol. Chem.* **2014**, *33*, 2609.
[26] T. Ozaki, T. Kimura, T. Ohnuki, Z. Yoshida, A. J. Francis, *Environ. Toxicol. Chem.* **2003**, *22*, 2800.
[27] X. Jin, Z. Chu, F. Yan, Q. Zeng, *Limnologica* **2009**, *39*, 86.
[28] P. Tai, Q. Zhao, D. Su, P. Li, F. Stagnitti, *Chemosphere* **2010**, *80*, 1031.
[29] F. Goecke, C. G. Jerez, V. Zachleder, F. L. Figueroa, K. Bisova, T. Rezanka, M. Vitova, *Front. Microbiol.* **2015**, *6*, 2.
[30] G. Santomauro, V. Srot, B. Bussmann, P. van, A. Aken, F. Brümmer, H. Strunk, J. Bill, *J. Biomater. Nanobiotechnol.* **2012**, *03*, 362.
[31] A. Buck, L. R. Moore, C. D. Lane, A. Kumar, C. Stroff, N. White, W. Xue, J. J. Chalmers, M. Zborowski, *J. Magn. Magn. Mater.* **2015**, *380*, 201.
[32] R. Brayner, C. Yepremian, C. Djediat, T. Coradin, F. Herbst, J. Livage, F. Fievet, A. Coute, *Langmuir* **2009**, *25*, 10062.
[33] R. Brayner, T. Coradin, P. Beaunier, J.-M. Greneche, C. Djediat, C. Yepremian, A. Coute, F. Fievet, *Colloids Surf., B* **2012**, *93*, 20.
[34] R. H. Crist, J. R. Martin, D. Carr, J. R. Watson, H. J. Clarke, *Environ. Sci. Technol.* **1994**, *28*, 1859.
[35] L. C. Rai, J. P. Gaur, *Algal Adaptation to Environmental Stresses*, Springer, Berlin **2001**.
[36] G. Santomauro, W.-L. Sun, F. Brümmer, J. Bill, *BioMetals* **2016**, *29*, 225.
[37] F. S. Richardson, *Chem. Rev.* **1982**, *82*, 541.
[38] K. Miazek, W. Iwanek, C. Remacle, A. Richel, D. Goffin, *Int. J. Mol. Sci.* **2015**, *16*, 23929.
[39] L. Kang, Z. Shen, C. Jin, *Chin. Sci. Bull.* **2000**, *45*, 585.
[40] Q.-G. Tan, G. Yang, K. J. Wilkinson, *Chemosphere* **2017**, *168*, 426.
[41] F. Goecke, V. Zachleder, M. Vítová, in *Algal Biorefineries* (Eds.: A. Prokop, R. K. Bajpai, M. E. Zappi), Springer International Publishing, Cham, Switzerland **2015**.
[42] P. R. Selvin, *Annu. Rev. Biophys. Biomol. Struct.* **2002**, *31*, 275.
[43] S. Pandya, J. Yu, D. Parker, *Dalton Trans.* **2006**, 2757.
[44] R. A. Mason, A. N. Mariano, *Chem. Geol.* **1990**, *88*, 191.
[45] Y. Kojima, M. Numazawa, S. Kamei, N. Nishimiya, *Int. J. Opt.* **2012**, *2012*, 1.
[46] N. W. Ashcroft, N. D. Mermin, *Festkörperphysik*, Oldenbourg, München **2013**.
[47] I. S. M. Khalil, M. P. Pichel, L. Zondervan, L. Abelmann, S. Misra, in *Springer Tracts in Advanced Robotics* (Eds: J. P. Desai, G. Dudek, O. Khatib, V. Kumar), Springer International Publishing, Heidelberg **2013**.
[48] H. Petermann, *PhD thesis*, Berichte, Fachbereich Geowissenschaften, Universität Bremen Nr. 56, **1994**.
[49] B.-W. Park, J. Zhuang, O. Yasa, M. Sitti, *ACS Nano* **2017**, *11*, 8910.
[50] I. Kolinko, A. Lohsze, S. Borg, O. Raschdorf, C. Jogler, Q. Tu, M. Posfai, E. Tompa, J. M. Plitzko, A. Brachmann, G. Wanner, R. Muller, Y. Zhang, D. Schuler, *Nat. Nanotechnol.* **2014**, *9*, 193.
[51] O. Garatun-Tjeldsto, H. Ottera, K. Julshamn, E. Austreng, *ICES J. Mar. Sci.* **2006**, *63*, 311.
[52] S. J. Fairweather-Tait, A. M. Minihane, J. Eagles, L. Owen, H. M. Crews, *Am. J. Clin. Nutr.* **1997**, *65*, 970.
[53] K. Wang, Y. Cheng, X. Yang, R. Li, *Met. Ions Biol. Syst.* **2003**, *40*, 707.
[54] M. Sitti, H. Ceylan, W. Hu, J. Giltinan, M. Turan, S. Yim, E. Diller, *Proc. IEEE* **2015**, *103*, 205.
[55] A. V. Singh, M. Sitti, *Curr. Pharm. Des.* **2016***22*, 1418.
[56] A. V. Singh, K. K. Mehta, K. Worley, J. S. Dordick, R. S. Kane, L. Q. Wan, *ACS Nano* **2014**, *8*, 2196.
[57] A. V. Singh, M. Batuwangala, R. Mundra, K. Mehta, S. Patke, E. Falletta, R. Patil, W. N. Gade, *ACS Appl. Mater. Interfaces* **2014**, *6*, 14679.
[58] A. V. Singh, M. Raymond, F. Pace, A. Certo, J. M. Zuidema, C. A. McKay, R. J. Gilbert, X. L. Lu, L. Q. Wan, *Sci. Rep.* **2015**, *5*, 7847.
[59] M. M. Stanton, B.-W. Park, D. Vilela, K. Bente, D. Faivre, M. Sitti, S. Sánchez, *ACS Nano* **2017**, *11*, 9968.
[60] H. Xu, M. Medina-Sánchez, V. Magdanz, L. Schwarz, F. Hebenstreit, O. G. Schmidt, *ACS Nano* **2018**, *12*, 327.
[61] Y. Alapan, O. Yasa, O. Schauer, J. Giltinan, A. F. Tabak, V. Sourjik, M. Sitti, *Sci. Rob.* **2018**, *3*, eaar4423.
[62] X. Yan, Q. Zhou, M. Vincent, Y. Deng, J. Yu, J. Xu, T. Xu, T. Tang, L. Bian, Y.-X. J. Wang, K. Kostarelos, L. Zhang, *Sci. Rob.* **2017**, *2*, eaaq1155.
[63] B. A. Rasala, S. P. Mayfield, *Bioeng. Bugs* **2011**, *2*, 50.